Control and Performance of the Rotational-to-Linear Cobotic Transmission

Eric L. Faulring* J. Edward Colgate† Michael A. Peshkin‡

Northwestern University§
Mechanical Engineering Department
2145 Sheridan Road, Evanston, IL 60208, USA

ABSTRACT

We examine the motion control bandwidth and stable impedance range of the Cobotic Hand Controller, a novel, six-degree-of-freedom, admittance controlled haptic display. A highly geared admittance architecture is often used to render high impedances with reasonable sized actuators for a haptic display. The Cobotic Hand Controller is perhaps the ultimate realization of an admittance display, since it is capable of obtaining an infinite gear ratio and can render infinite impedances (up to its own structural stiffness). The incorporation of continuously variable transmissions in the Cobotic Hand Controller provides for an extremely wide, stable z-width, since the transmission ratio can be adjusted quickly to vary the backdrivability. However, finite preloads in the transmissions limit the display's acceleration capabilities. We examine the control challenges and performance characteristics of the Cobotic Hand Controller for free motion and unilateral impact virtual environment scenarios.

CR Categories: H.5.2 [Information Systems]: Information Interfaces and Presentation—User Interfaces

Keywords: haptics, cobots, z-width, rotational-to-linear transmission

1 INTRODUCTION

Cobots, or collaborative robots, utilize the rolling constraints of wheels in their transmissions to relate the relative motion of joints [9, 14]. These passive mechanical constraints yield devices that are safe and stable for interaction with human operators, and allow for haptic displays that utilize small motors and very little electrical power. The Cobotic Hand Controller (Figure 1) is a recently introduced six-degree-of-freedom cobotic haptic display [7]. Its ability to render high-degree-of-freedom bilateral constraints has been demonstrated [8]. The device's use of continuously variable transmissions and a parallel architecture imparts structural stiffness of 50 kN/m and the capability to sustain 50 N loads while using only a few watts of electrical power. Unlike previous cobots, this device has reasonable unilateral performance, a consequence of the rigid transmissions and relatively high bandwidth that result from the use of steel elements in rolling contact.

The design of the six-degree-of-freedom Cobotic Hand Controller (Figure 2), utilizes the kinematics of the parallel platform introduced by Merlet [11]. The proximal links are coupled to the distal links by three-degree-of-freedom universal joints. The distal links are in turn are coupled to an end-effector platform via two-degree-of-freedom universal joints. A force sensor is placed at the end-effector to help determine the user's intent. We have modified Merlet's kinematics coupling the six linear actuators to a central power cylinder through non-holonomic rolling constraints. Our six-degree-of-freedom device has six steering motors and one additional motor drives the cylinder.

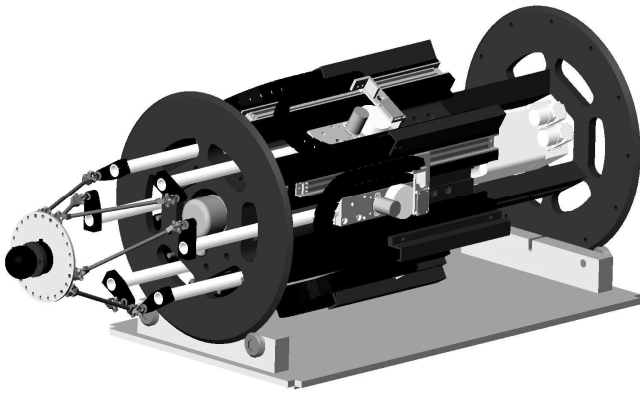

Figure 1: A CAD rendering of the Cobotic Hand Controller haptic display. The operator interacts with the spherical manipulandum at left.

Linear actuation of the proximal links is achieved via a rotational-to-linear continuously variable transmission (CVT), a steered wheel. A linearly moving carriage contains the CVT wheel, steering motor, rotational encoder and linear potentiometer wiper, and is the attachment point for the base of each proximal link. The angle of each wheel, ϕ_i, relates the linear velocity $\dot{l}_i$ of each proximal link to the rotational velocity of the power cylinder. The six rolling constraints determine the direction of a single motion freedom for the end-effector, and the cylinder motor controls motion along this direction. When the wheels are steered such that their rolling axis is parallel to the power cylinder ($\phi_i = 0$), a ratio $\dot{l}_i = -R\omega\tan\phi_i = 0$ is set. Steering the wheels either direction from $\phi_i = 0$ results in ratios between $\pm$ infinity. However, in practice, wheel slip limits this range. Turning all six wheels to $\phi_i = 0$ locks the six actuators, and turning them to $\phi_i = \pi/2$ completely decouples the actuators from the cylinder's velocity, preventing the cylinder from turning.

The Cobotic Hand Controller utilizes a parallel architecture that contains a control redundancy. It has one more actuator than task-space degrees of freedom (Figure 3). Others have addressed this control redundancy via various techniques [10, 12, 15]. We designed a controller that varies the common element speed with respect to the sum of kinetic and potential energy in the virtual environment [6]. Although there are many benefits to varying the cylinder speed dynamically, the analysis presented here uses a fixed-speed cylinder controller in order to simplify discussion and analysis of other issues.

*e-mail:e-faulring@northwestern.edu
†e-mail:colgate@northwestern.edu
‡e-mail:peshkin@northwestern.edu
§This work was supported by the DOE grant number DE-FG07-01ER63288.

Symposium on Haptic Interfaces for
Virtual Environment and Teleoperator Systems 2006
March 25 - 26, Alexandria, Virginia, USA
1-4244-0226-3/06/$20.00 ©2006 IEEE

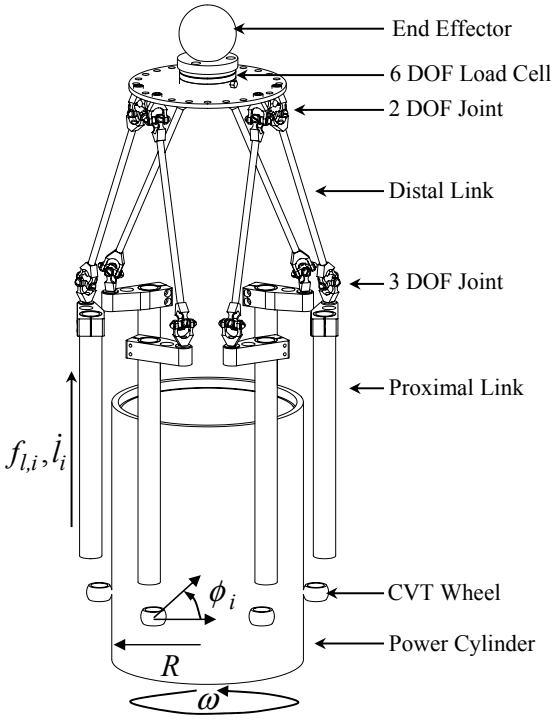

Figure 2: The kinematics of a Merlet-Cobotic parallel platform. This design consists of six linear actuators arrayed around a central power cylinder. Steered wheels loaded against the cylinder act as continuously variable transmissions, and relate the translational joint velocities to the cylinder's angular velocity. The carriages coupling the wheels to the proximal links, as well as the linear guideways for the joints have been removed for clarity.

A description of the mid and low level controllers utilized to steer the Cobotic Hand Controller's transmissions, drive its cylinder, and provide feedback control of the Cobotic Hand Controller joint motions is provided below. We examine the resulting motion control bandwidth of the device, demonstrate the acceleration capability during unilateral impacts, and analyze the stable virtual environment z-width for interaction with various impedances.

2 Control of the Cobotic Hand Controller

The Cobotic Hand Controller is operated as an admittance display as diagrammed in Figure 4. A load cell measures the operated applied forces and the torques that are used by a virtual environment model to compute desired accelerations. The virtual environment framework we use is described in [6, 8]. The cobot then renders these motions via three separate feedback controllers. These include a joint motion controller, a steering velocity controller, and a cylinder velocity controller. We drop the subscript i notation that indicates an individual joint for the remainder of this paper. We will not discuss the kinematics relating the $\mathbb{R}^6$ coordinate representation of the virtual environment to the $SE(3)$ task space of the display's end-effector, nor the kinematics relating task space to the linear motions of the joints described elsewhere [6, 8]. The remainder of the analysis assumes a single joint cobot with two actuators (one steering and one cylinder) and one output (the single linear joint).

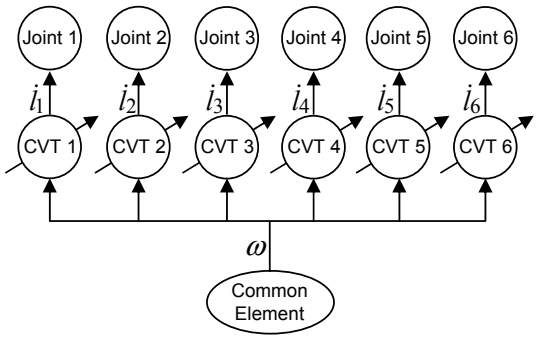

Figure 3: While there are six joint speeds that must be controlled to render a virtual environment, there are also six CVTs and a cylinder that must be actuated. The cylinder speed is arbitrary since it is related via the CVTs to the joints.

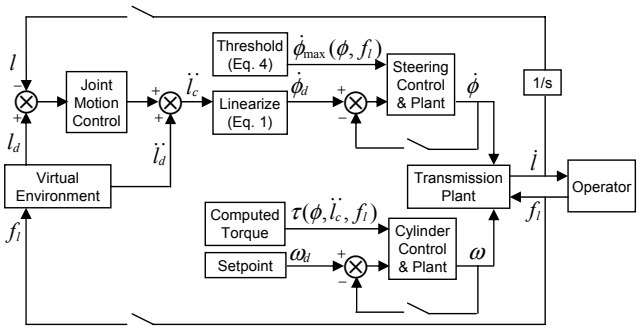

Figure 4: The interaction force f_l between the operator and the cobot is measured, and is the input to a high-level virtual environment model. The output of this model, desired motion $\ddot{l}_d$, is assured by a mid-level joint motion controller. The actual motion of the cobot, $\dot{l}$, is mediated by steering and cylinder plants, each containing their own low-level feedback controllers.

2.1 Joint control

The joint motion controller (see Figure 4) uses $\ddot{l}_d$ from the virtual environment model as a feedforward component. A PID feedback component augments the feedforward acceleration via a proportional feedback term on error, $e = l_d - l$, a derivative term, $\dot{e} = \dot{l}_d - \dot{l}$, and an integral term, $\int e dt$. The result is a nominal joint acceleration command $\ddot{l}_c$. This is converted to a desired steering velocity via the joint to steering kinematics (Equation 1).

$$\dot{\phi}_d = -\frac{\ddot{l}_c + R\dot{\omega}\tan(\phi)}{R\omega\sec^2\phi} \tag{1}$$

2.2 Steering control

The CVT steering velocity, $\dot{\phi}$, is maintained via a separate proportional plus integral (PI) feedback controller. The current implementation of the closed loop steering velocity controller has 100 Hz bandwidth.

2.3 Cylinder control

The CVTs draw velocity from a cylinder that is driven at a desired speed by a proportional plus integral (PI) feedback controller. In the current implementation, the surface speed of the cylinder is fixed at 0.34 m/s. We elaborate upon selection of cylinder speed, as well

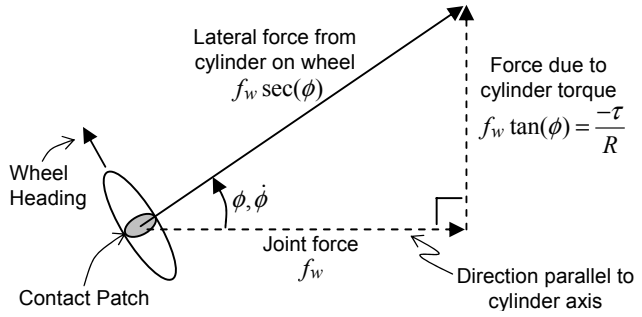

Figure 5: The lateral force at the contact patch of the wheel/cylinder interface is resolved into the cylinder and joint efforts. The wheel does not sustain a longitudinal force, as nothing restrains the wheel from spinning about its axle.

as controllers that dynamically vary the speed of the cylinder, elsewhere [6]. A computed torque feedforward term predicts the cylinder torque, τ, required to accelerate joint masses and match the operator applied force. The current implementation of the closed loop cylinder velocity controller has 70 Hz bandwidth.

3 Origins of Performance Limitations

An analysis of the forces at the contact patch of the wheel is critical for determining the performance limits of the Cobotic Hand Controller. Here we delineate two state-dependent performance limits due to finite preload force. The first limits the static output force of the joint, and the second the acceleration capability of the joint.

The sources of lateral force on the wheel are depicted in Figure 5. The lateral force on the wheel, $f_w \sec(\phi)$, can be resolved into the output force of the joint at the wheel, f_w, and the force of the cylinder, $f_w \tan(\phi)$, due to cylinder torque, τ. The output force of the joint at the wheel (Equation 2), is composed of the inertial force of the joint, $m\ddot{l}$, the joint friction force, $cPsgn(\dot{l})$, and the net output force of the joint, f_l. Forces in the longitudinal (rolling direction) of the wheel are essentially zero.

$$f_w = m\ddot{l} + cPsgn(\dot{l}) - f_l \tag{2}$$

f_l is the operator applied force and c is the linear guideway dynamic coefficient of Coulomb friction. For preload force P set to 250 N, $cP = 0.84$ N. The joint masses m are 0.9 kg.

3.1 Limited joint force

The net lateral force on the wheel, $f_w \sec\phi$, is of primary concern. Adequate lateral friction force, μP, must be present to provide f_w (Equation 3).

$$f_w \leq \frac{\mu P}{\sec\phi} \tag{3}$$

When Equation 3 is satisfied, adequate friction force is available to accelerate the linear carriage, to combat joint friction and to apply the net force, f_l, to an operator. The coefficient of friction between the steel wheels and steel cylinder, $\mu \approx 0.12$, has been determined experimentally.

3.2 Limited joint acceleration

We also derive a method to prevent slip based instabilities in the transmission by limiting joint acceleration. Acceleration of the joint inertia requires significant forces from the wheel. Joint acceleration can be limited by controlling $\dot{\phi}$. A constraint on $\dot{\phi}$ is established by solving Equation 2 for $\ddot{l}$ and substituting into Equation 1 and setting

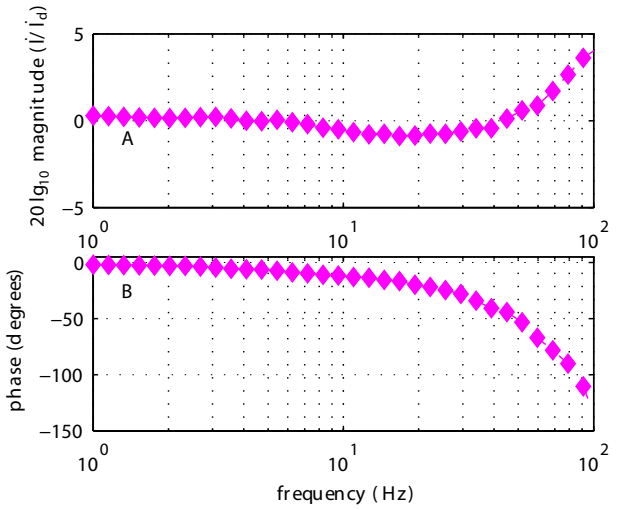

Figure 6: Frequency response of the closed loop joint motion control. The system has 45 degrees of phase lag at 40 Hz bandwidth. Virtual environments must only contain frequency content below 40 Hz in order to be guaranteed stable.

$\dot{\omega} = 0$. The result is a maximum steering velocity given the current angle, cylinder speed, joint mass and operator force (Equation 4).

$$\dot{\phi}_{max}(\phi) = \frac{\frac{\varepsilon\mu P}{\sec(\phi)} - cPsgn(\dot{l}) + f_l}{mR\omega\sec^2(\phi)} \tag{4}$$

f_w has been replaced by $\varepsilon\mu P$, a fraction ε of the available friction force in order to avoid approaching the gross slip regime of the rolling contact transmission. If the measured steering velocity exceeds the limit from Equation 4, the steering torque command from the steering velocity controller is pulled to zero. This limit has been implemented with $\varepsilon = 0.5$ and works well at preventing creep or gross-slip based instabilities in the transmission.[1] The joint friction and operator force components of Equation 4 were ignored during implementation since the these loads are small relative to the carriage inertial loads in our implementation.

4 Performance

4.1 Motion control bandwidth

In Figure 6, we plot the closed loop bandwidth of the complete joint motion controller and joint plant. The force sensor does not contact anything for this experiment. The system is driven by commanding a desired acceleration, $\ddot{l}_d = 1.0\sin(2\pi ft)$, at each of 33 frequencies spaced logarithmically from 1 to 100 Hz. Desired velocity and position, $\dot{l}_d = 2\pi f\cos(2\pi ft)$ and $l_d = -4\pi^2 f^2\sin(2\pi ft)$, are used for the feedback joint motion component. Ideally the closed-loop frequency response would be a flat line at 0 dB that rolled off at some frequency, however the gain of experimental response rises above unity as 100 Hz is approached. This is due to both a resonance in the steering plant around 100 Hz and to the fact that the obtainable amplitude of linear motion at these frequencies is too small for the sensors to accurately measure for feedback purposes. We were unable to input larger desired motion at high frequencies since the steering actuator torque limits would be exceeded. The

[1] Lateral creep occurs due to the elastic properties of the rolling wheel, while gross-slip occurs due to exceeding the coefficient of friction. These are discussed in greater detail in regards to this device in Faulring [6].

frequency response of the joint motion control system has 0 dB of attenuation through 40 Hz, where phase lag is limited to 45 degrees.

The experiment was performed at a cylinder surface speed of 0.34 m/s. Performing this experiment at different cylinder surface speeds (or with another type of controller that varied the cylinder speed) may require more or less steering torque and steering excursion, however, the magnitude and phase plots of linear motion bandwidth would be identical if the required steering torque does not saturate. Although the relationship between steering velocity and linear motion is nonlinear, we have incorporated this (Equation 1) into the controller so that the dynamics of our joint motion controller are linear regardless of the cylinder surface speed or transmission angle.

4.2 Acceleration capability

In Figure 7, the performance of the Cobotic Hand Controller is analyzed during impact with a unilateral virtual environment constraint. The virtual environment mass is 2 kg and the wall stiffness and damping are 10,000 N/m and 400 N(s)/m, respectively. The experiment is executed by the operator holding the end-effector loosely with all five fingers as he bangs it sequentially into the constraints at $l = \pm 30$ mm (Subplot A). Attention is given to obtaining approximately the same pre-impact velocity for each impact. In Subplot B the actual penetration versus the desired penetration is displayed. The desired trajectory penetrates the walls only about 1.0 mm while the actual penetration is 4.5 mm. The simulation requires a 34 m/s^2 deceleration but only a 7.4 m/s^2 deceleration is actually rendered. This is a consequence of the limited acceleration capability of the device and is not a bandwidth limitation. The current implementation is capable of $\frac{\mu P}{m}$ = 30 m/s^2 acceleration[2], but the steering velocity limit (Equation 4) set to 15 m/s^2 and other controller dynamics limit the actual closed loop performance. The result is that constraints are initially soft but harden quickly after the impact, quite the opposite of impulse controlled impedance displays that can "punch" a user to stop initial penetration, but cannot sustain significant loads.

4.3 Stable impedance range

We establish the range of virtual admittances or impedances that the cobot can stably render, the z-width of the Colgate and Brown [3, 1], as a function of the mechanical impedance the end-effector contacts. Figure 8 depicts the method by which the data is obtained for this experiment. The virtual environment of the system consists of a virtual spring, $k_{virtual}$, a virtual damper, $b_{virtual}$, and a virtual mass, $m_{virtual}$. If the actual cobot and virtual systems move to locations, $x_{physical}$, and $y_{virtual}$, the real spring, $k_{physical}$, generates a load, f_{sensor}, at the load cell. Similar testing protocols are implemented by others for determining the stable impedance range of a haptic display [2, 4, 5, 13]. The simulation is oriented along the axis of the cylinder, rendering the motion of all six joints identical. The experiment was performed with the nominal cylinder surface speed set at 0.34 m/s, and with the maximum steering velocity heuristic actively limiting steering torque if $\dot{\phi}_{max}$ was to be exceeded. The test protocol required the end-effector to be brought into contact with the real spring by moving parallel to the axis of the cylinder at 5 cm/s until a 5 N load was detected. The zero point of the virtual spring was set at this location. After a 0.25 second delay, the virtual environment simulation was started and a stability metric applied.

[2]This has been verified by turning off the steering velocity heuristic, and driving the joint with low frequency large amplitude motions. Without any high frequency content or commanded accelerations greater than 30 m/s^2, no gross slip occurs, although significant lateral creep of the wheel is observed.

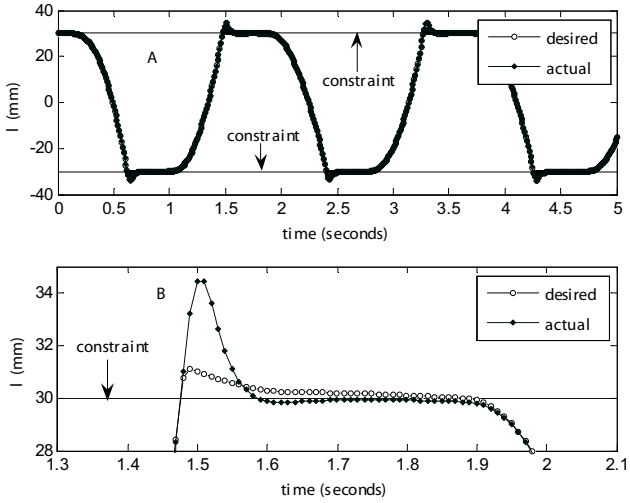

Figure 7: A. The user is moving the end-effector between unilateral constraints located at ±30 mm. B. The actual and desired penetrations of the constraint are depicted for a single impact.

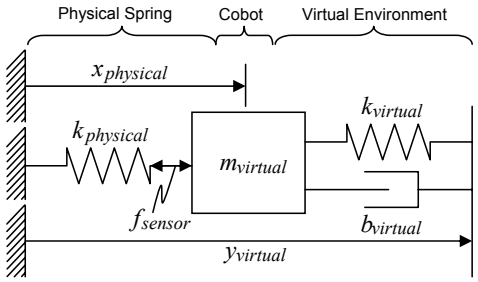

Figure 8: Schematic of admittance display system. The virtual environment gives the desired impedance, or interaction behavior of the cobot with the physical environment.

We tested 4 different virtual masses over a range of virtual damping and virtual stiffness. In addition, the whole experiment was performed with three different physical springs, $k_{physical}$. The first spring was a 1000 N/m die spring, approximately 30 cm long and 3.5 cm in diameter, slid onto a cylinder for support as it lay horizontally. The second spring was a 3000 N/m die spring, also 30 cm long and 3.5 cm in diameter, and again slid onto a cylinder for support as it lay horizontally. The third was a 6000 N/m piece of 12 mm thick, 40 durometer polyurethane. The stability metric and exploration algorithm are explained in greater detail in Faulring [6].

In Figure 9 we plot the results of the z-width exploration tests. Figure 9 shows the stable virtual stiffness/damping regimes for the three physical springs examined. Depending on the impedance of the physical system that the Cobotic Hand Controller is interacting with, the stable virtual impedances it can render are characterized by a top stable natural frequency between 15 and 40 Hz (if we form a second order system from $m_{virtual}$, $k_{virtual}$ and $b_{virtual}$). Regardless of the impedance, $k_{physical}$, that the end-effector contacted, increasing the mass, $m_{virtual}$, always led to higher stable stiffness, $k_{virtual}$, and to a larger range of stable values for damping, $b_{virtual}$. The minimum useful virtual environment impedance is around 2 kg with zero damping, although a "careful" user is capable of manipulating a 0.1 kg mass with zero damping. The 2 kg mass need not have any weight (zero virtual gravity), so the operator only feels

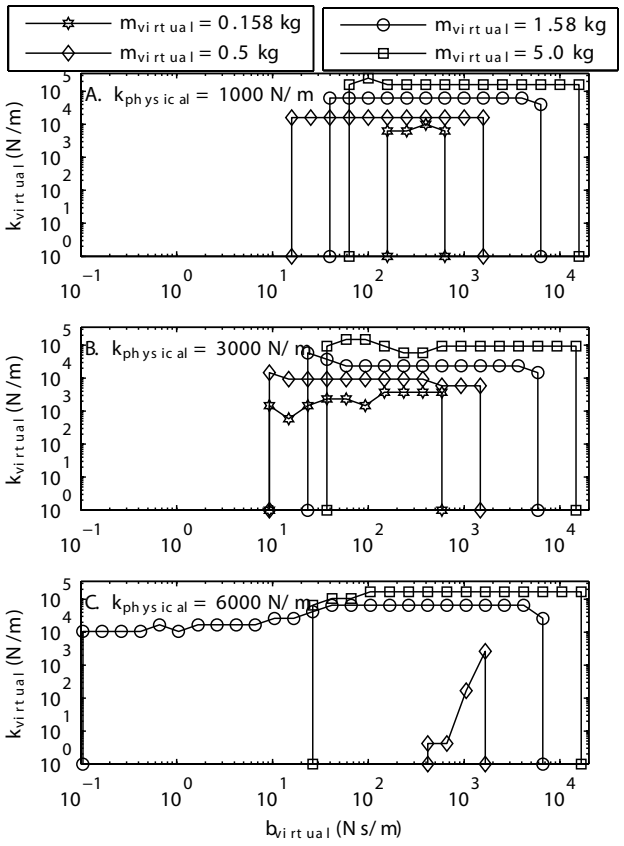

Figure 9: Stability regime in the virtual stiffness and virtual damping plane for various virtual inertias. A. Physical impedance $k_{physical}$=1000 N/m die spring. B. Physical impedance $k_{physical}$=3000 N/m die spring. C. Physical impedance $k_{physical}$=6000 N/m 40 durometer polyurethane pad. There were no stable points for $m_{virtual}$ = 0.158 kg with the polyurethane. If the structural stiffness of the Merlet platform is taken into account, these 100 kN/m software levels may in actuality only be 20 to 40 kN/m, depending on configuration.

the inertial forces which are small for low accelerations. When controlled by a human, the virtual environment properties are usually a 2 kg mass with damping 0.1 N(s)/m.

Although the dynamic range of the Cobotic Hand Controller is high (the ability to simulate a < 2 kg mass with zero damping and the ability to sustain 50 N loads while defending 100 kN/m constraints), the stable impedance range is limited by steering dynamics and transmission slip. Steering dynamics produce a phase lag of joint motion relative to virtual environment motions that tends to help filter out high frequency content from transmitting from the virtual environment to the joint motion. More detrimental is the slip that occurs in the transmission when the inertial force incurred by attempting to accelerate/decelerate a joint is in excess of the friction force due to preload. This slip causes a deviation between the desired and measured motions, and large feedback errors are generated that require even larger steering velocities, initiating a positive feedback loop. In addition, the high frequency content of a slip occurrence will excite the structural resonances of the proximal and distal links. The maximum steering velocity heuristic introduced earlier prevents such instabilities.

5 Conclusion

We have demonstrated the ability of an active cobot to control motion in excess of 40 Hz and to render unilateral contacts involving accelerations of 30 m/s^2. We have also demonstrated the Cobotic Hand Controller's broad stable impedance range, characterized by virtual mass as low as 0.158 kg and virtual stiffness as high as 100 kN/m. The typical virtual environment properties used in simulations of free space are a 2 kg mass and damping 0.1 N(s)/m, while constraints are typically characterized by stiffness 10 kN/m and damping 400 N(s)/m. The use of cobotic continuously variable transmissions in the Cobotic Hand Controller, constructed with steel elements in rolling contact, allows this admittance controlled haptic display to achieve a high dynamic range.

References

[1] J.M. Brown and J.E. Colgate. Minimum mass for haptic display simulations. In *ASME IMECE DSC*, pages 249–256, 1998.

[2] J.E. Colgate. *The control of dynamically interacting systems*. Ph.D. Dissertation, Massachusetts Institute of Technology, 1988.

[3] J.E. Colgate and J.M. Brown. Factors affecting the Z-width of a haptic display. In *IEEE International Conference on Robotics and Automation*, pages 3205–3210, San Diego, CA, 1994.

[4] R.E. Ellis, O.M. Ismaeil, and M. Lipsett. Design and evaluation of a high-performance haptic interface. *Robotica*, 14(3):321–327, 1996.

[5] S.D. Eppinger. *Modelling robot dynamic performance for endpoint force control*. Ph.D. Dissertation, Massachusetts Institute of Technology, 1988.

[6] E.L. Faulring. *The cobotic hand controller: Design, control and analysis of a novel haptic display*. Ph.D. Dissertation, Northwestern University, 2005.

[7] E.L. Faulring, J.E. Colgate, and M.A. Peshkin. A high performance 6-DOF haptic cobot. In *IEEE International Conference on Robotics and Automation*, pages 1980–1985, New Orleans, LA, 2004.

[8] E.L. Faulring, K.M. Lynch, J.E. Colgate, and M.A. Peshkin. Haptic interaction with constrained dynamic systems. In *IEEE International Conference on Robotics and Automation*, Barcelona, Spain, 2005.

[9] R.B. Gillespie, J.E. Colgate, and M.A. Peshkin. A general framework for cobot control. *IEEE Transactions on Robotics and Automation*, 17(4):391–401, 2001.

[10] S. Kim. *Control of the powered arm cobot and analysis of the rotational CVT*. Ph.D. Dissertation, Northwestern University, 2003.

[11] J.P. Merlet. Direct kinematics and assembly modes of parallel manipulators. *International Journal of Robotics Research*, 11(2):150–162, 1992.

[12] C.A. Moore. *Design, construction, and control of a 3-revolute arm cobot*. Ph.D. Dissertation, Northwestern University, 2001.

[13] M. Moreyra and B. Hannaford. A practical measure of dynamic response of haptic devices. In *International Conference on Robotics and Automation*, pages 369–374, Leuven, Belgium, 1998.

[14] M.A. Peshkin, J.E. Colgate, W. Wannasuphoprasit, C.A. Moore, R.B. Gillespie, and P. Akella. Cobot architecture. *IEEE Transactions on Robotics and Automation*, 17(4):377–390, 2001.

[15] J.J. Santos-Munné. *Extreme joystick: A cobot with stored energy*. Ph.D. Proposal, Mechanical Engineering Department, Northwestern University, 1997.